Single-slit diffraction of the arbitrary vector beams

Sixing Xi (席思星), Xiaolei Wang (王晓雷)*, Qiang Wang (王 强), Shuai Huang (黄 帅), Shengjiang Chang (常胜江), and Lie Lin (林 列)

Institute of Modern Optics, Key Laboratory of Optical Information Science and Technology, Ministry of Education, Nankai University, Tianjin 300071, China

*Corresponding author: xisixing@126.com

Received July 30, 2014; accepted November 14, 2014; posted online January 5, 2015

We present the single-slit diffraction of the arbitrary vector fields with different parameters m, n, and φ_0 theoretically and experimentally. The single slit covers the polarization singularity in the center and therefore the influence of the polarization singularity on the diffraction fringes is analyzed. The experimental results which agree well with the simulation results show that the total intensity of the diffraction field is related only to the topological charge m, but the polarization distribution of the diffraction field is related to all the parameters m, n, and φ_0. Therefore, the diffraction patterns allow to determine all the parameters of the arbitrary vector fields.

OCIS codes: 230.3720, 260.5430, 120.5060.
doi: 10.3788/COL201513.012302.

The homogeneous or inhomogeneous state of polarization of light is one of the most fundamental properties of the electromagnetic field. This important property is widely used in various fields, such as optical imaging[1], particle trapping[2], particle manipulation[3], and nonlinear optics[4]. Especially, when the reliable and flexible method of generating arbitrary vector beams was proposed by Wang *et al.*[5] and the method is improved to generate an arbitrary space-variant vector beam with structured polarization and phase distributions[6]. There are many studies on the effects and the application of the vector beams[7–10], for instance, the peculiar interference behaviors of the vector fields in Young's two-slit configuration was given by Li *et al.*[11], and the results have potential applications such as characterizing the topological properties of the arbitrary vector fields. But Young's two-slit configuration blocked the polarization singularity of the vector beams, while the polarization singularity is the important part of the vector beam and have important applications in the precise measurement of the deformation and displacement of submicrometer particles and life science research[12–14]. Besides, the motion of polarization singularities takes place by varying waist width ratio, amplitude ratio, and propagation distance[15], especially in the paraxial[16,17] and diffraction conditions[18,19]. Diffraction has been employed extensively to reveal the unusual phase distribution of the phase singular beam[20]. In order to design optical components and imaging systems using vector beams, the single-slit diffraction of the arbitrary vector beams is applied to explain the phase and other characteristics, in particular, phase and other characteristics containing the polarization singularity of the arbitrary vector beams.

In this letter, we explore the single-slit diffraction of the arbitrary vector fields theoretically and experimentally. The method of generating arbitrary vector beams proposed in Ref. [5] is applied in this letter and the final vector beams are synthesized from the left- and right-hand polarized beams which load the phases with special spatial distribution. Thus, the diffraction patterns of these fields are firstly observed, because there are many novel effects of the interference in the double slit[21] and diffraction in the single slit[22]. The results show that the polarization singularity at the center of the light has a great influence on the diffraction pattern. Because the single-slit diffraction patterns structure carry the information of the phase and polarization distributions of the arbitrary vector field, so the structure and polarization distribution of the diffraction patterns will also unveil the characteristics of the arbitrary vector light field. Besides, our research on the phenomenon of vector near-field diffraction has a guiding significance for the study of the limited transmission[23], the spatial and temporal evolutions of the vector optical field[24], and the interaction of vector light with matter[25].

The field distribution of the single-slit diffraction results from the interference of the coherent light and the fringe distribution is determined by the phase distribution. It is noticed that the arbitrary vector beams in our experiment are the superpositions of two orthogonal circularly polarized beams. Firstly, we propose the single-slit diffraction of the left- and right-hand circularly polarized beams carrying phase which controls the polarization of the vector beams.

In the method, the phase loading on the spatial light modulator is $\delta = m\varphi + 2n\pi\rho/\rho_0 + \varphi_{0,}$ −1 order diffraction light modulated for left-hand polarized beam of unit amplitude illuminates the narrow slit, and the field just behind the slit is given by

$$u^{-1} = \mathrm{rect}\left(\frac{x}{b}\right)\exp[\mathrm{i}(m\phi + 2n\pi\rho/\rho_0 + \phi_0)], \tag{1}$$

where b is the slit width, ρ_0 is the radius of the arbitrary vector field and initial phase φ_0, while m and n are the indices of the angular and radius, respectively.

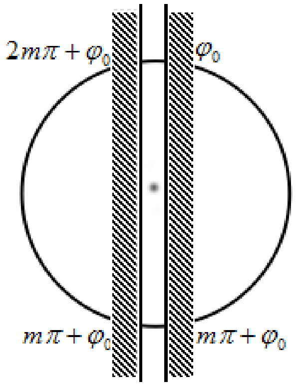

Fig. 1. Field just behind the slit of the left-hand polarized beam.

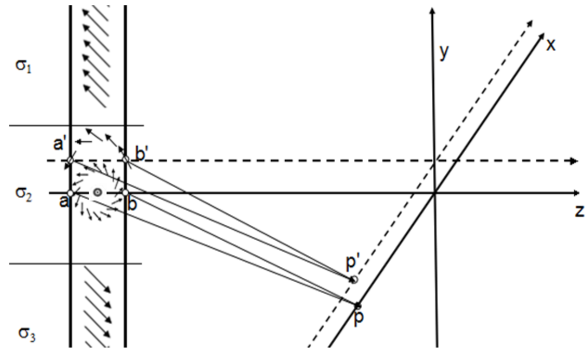

Fig. 2. Analysis of the polarization state in the slit.

Accordingly, diffracted +1 order light modulated for right-hand polarized beam illuminates the narrow slit, and the field just behind the slit is

$$u^{+1} = \mathrm{rect}\left(\frac{x}{b}\right)\exp[-\mathrm{i}(m\phi + 2n\pi\rho/\rho_0 + \phi_0)]. \tag{2}$$

Figure 1 shows the field just behind the slit of the left-hand polarized beams, where the white circular spot represents the arbitrary vector beam. The single slit is in the middle covered by the polarization singularity. The phase on different positions of the single slit is marked in Fig. 1, where the phase $2n\pi\rho/\rho_0$ is ignored, which only changes the phase distribution in vertical direction.

For the plane wave, the phase in the slit has uniform distribution. So the diffraction fringes are parallel to the slit and have sinc^2 intensity distribution[10] as

$$I = I_0\frac{\sin^2\beta}{\beta^2};\beta = \frac{\pi}{\lambda}b\sin\alpha, \tag{3}$$

where β represents the phase difference between the waves reaching the point of observation from two points in the slit and α is the diffraction angle. For the plane wave, the phase in the slit is the same, so the straight fringes will appear in the diffraction pattern. For the phase difference caused by path difference between the interfering waves at any point, the arbitrary vector beams remain the same as a uniform plane wave, but will change the phase distribution in the plane just behind the slit.

Thus, when an arbitrary vector beam illuminates the slit, the intensity pattern will be a sinc^2 distribution on the whole. But owing to the change in the phase distribution, the value of β will be modified as

$$\beta' = \frac{\pi}{\lambda}b\sin\alpha + \gamma, \tag{4}$$

where γ is the additional phase due to the non-uniform phase distribution of the arbitrary vector beam in the slit, and can be given by phase change along left and right edges of the slit.

Here the width of the slit is considered to be infinitely small, so the relative phase distribution in the bottom of the slit is uniform plane, whereas $2m\pi$ is added in the upper portion because of the abrupt phase. However, the relative phase distribution changes largely in the center where the polarization singularity is located as shown in Fig. 2.

In order to compute the additional phase γ, we write the complex amplitude of +1 order diffraction beam as

$$u(x,y) = (x+\mathrm{i}y)^m = r^m\exp(\mathrm{i}\delta(x,y)), \tag{5}$$

where $\delta(x, y) = m\varphi + \varphi_0 = \arg[(x+\mathrm{i}y)^m]$. Equation (5) can be solved as

$$\delta(x,y) = m\phi + \phi_0 = \frac{m}{\mathrm{i}}\ln\left[\frac{x+\mathrm{i}y}{\sqrt{x^2+y^2}}\right] + \phi_0. \tag{6}$$

As shown in Fig. 1 we obtain the additional phase γ along y from Eq. (6) by setting $x = -b/2$ and $x = b/2$ as

$$\gamma = \delta_l - \delta_r = \frac{m}{2\mathrm{i}}\ln\left(\frac{-(b/2)+\mathrm{i}y}{b/2+\mathrm{i}y}\right). \tag{7}$$

Therefore, we divide the whole into three portions, σ_1 in the upper, σ_3 in the bottom, and σ_2 in the center. In this case, in the top σ_1 and the bottom σ_3 portions, γ values are $2m\pi$ and 0, respectively. In the center σ_2 portion, the value of γ varies continuously from 0 to $2m\pi$.

Therefore, we can consider that the diffraction fringes in σ_1 and σ_3 regions are parallel to the slit. Because of the additional phase $2m\pi$, there will be displacement of the diffraction fringes in the upper and bottom portions. The bright fringes are where $\sin\beta = 1$ can be deduced from Eq. (3). In other words, the bright fringes in the bottom are near $\beta_i = \pm i\pi + \pi/2$ where i is constant. But in the upper portion, bright fringes are near $\beta_i = -2m\pi \pm i\pi + \pi/2$, so there are $2m\pi$ differences for them in the upper and lower halves of the slit. But in the middle σ_2 portion, the value of γ varies continuously from 0 to $2m\pi$, so each bright fringe in the upper half portion bends near the center and joins the mth bright fringe to the left in the bottom. Certainly, if opposite topological charge $-m$ is used, the bending will take place in the opposite direction and there will be two opposite phenomena in both cases for ±1 order diffraction beams.

But for the distribution of the stripe observed on the CCD, the displacement for the fringe will also be influenced a lot by a and b, where a is the diffraction distance. It is well-known that there will be dark fringes when $\beta = b\pi\sin\alpha/\lambda = \pm\pi, \pm 2\pi, \pm 2\pi, \ldots$ in the bottom, it means $\sin\alpha_i = \pm i\lambda/b$. We can consider the diffraction angle $\alpha_i = \pm i\lambda/b$ in paraxial approximation. So the dark fringe of the diffraction will present at $x_i = \pm ia\lambda/b$, but it is $x_i = \pm(m+i)a\lambda/b$ for the upper portion of the fringes. So the displacement is $\tau_x = \pm ma\lambda/b$, and the symbol + expresses that the fringes bends to right, whereas the symbol − is the opposite.

In our experiment, we can deem that the left- and right-hand polarized beams are not coherent, so the total intensity of the single-silt diffraction field is the superposition of that of the left- and right-hand polarized beams. Therefore, the intensity of the single-slit diffraction field can be given as

$$I = I_{-1} + I_{+1} = \frac{1}{2}\left(I_0 \frac{\sin^2 \beta'_{-1}}{{\beta'_{-1}}^2} + I_0 \frac{\sin^2 \beta'_{+1}}{{\beta'_{+1}}^2}\right). \tag{8}$$

On the basis of above theories and the Huygens–Fresnel principle, the polarization distribution of single-slit diffraction field in Fig. 2 can be analyzed as follows. In the σ_1 region, the polarization distribution can be considered constant across the narrow slit, so the diffraction patterns of the x-component can be given as

$$I_x = I_{-1}\cos^2\theta + I_{+1}\cos^2(-\theta), \tag{9}$$

where θ is the polarizing angle when $\varphi = 0$. In the same way, the y-component is

$$I_y = I_{-1}\sin^2(-\theta) + I_{+1}\sin^2\theta. \tag{10}$$

It is also the same in the σ_3 region but θ is the polarizing angle when $\varphi = \pi$. In the σ_2 region, the polarization state changes largely, but in order to analyze this polarization distribution, the approximation can be given as

$$\begin{aligned} I_x^{(y=y_0)} &= c_1^{(y=y_0)} I \left(\cos^2\theta^{\left(x=\frac{b}{2},y=y_0\right)} + \cos^2\theta^{\left(x=\frac{-b}{2},y=y_0\right)}\right) \\ &= c_2^{(y=y_0)} I \cos^2\theta^{\left(x=\frac{b}{2},y=y_0\right)}, \end{aligned} \tag{11}$$

$$\begin{aligned} I_y^{(y=y_0)} &= c_1^{(y=y_0)} I \left(\sin^2\theta^{\left(x=\frac{b}{2},y=y_0\right)} + \sin^2\theta^{\left(x=\frac{-b}{2},y=y_0\right)}\right) \\ &= c_2^{(y=y_0)} I \sin^2\theta^{\left(x=\frac{b}{2},y=y_0\right)}, \end{aligned} \tag{12}$$

where $c(y=y_0)$ is constant which means approximate.

We now experimentally explore the single-slit diffraction of the arbitrary vector field. The arbitrary vector beam is experimentally generated using He–Ne laser at 632.8 nm as the light source. The created vector field falls normally on the slit with $b = 0.2$ mm, but the diffraction distance is not a fixed value which will be changed as the complexity of the diffraction patterns. A polarizer can be inserted between the slits and CCD, so the diffraction patterns of the x- and the y-components

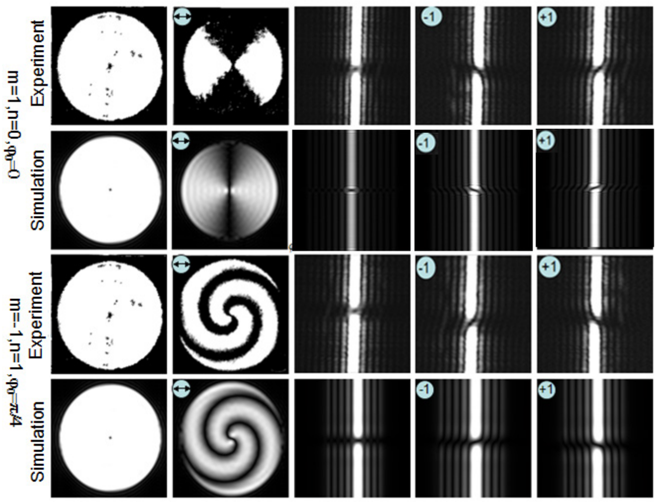

Fig. 3. Experimental and simulation results of the single-slit diffraction patterns of vector field with $m=1$, $n=0$, $\varphi_0=0$, and $m=-1$, $n=1$, $\varphi_0=0$.

will be acquired. According to the analysis of Fig. 2, the stripe displacement of the upper and lower parts in the diffraction field is $\tau_x = \pm ma\lambda/b$, which is 0.63–1.20 mm in our experimental conditions ($b=0.1$ mm, $a=10$–30 cm), and the displacement can be observed in our CCD (576×768 pixels, 6×8 (mm)).

Firstly the single-slit diffraction patterns with different arbitrary vector beams are observed as shown in Fig. 3. The first row shows the field distribution through the horizontal polarizer and the diffraction patterns of the vector fields with $m = 1$, $n = 0$, $\varphi_0 = 0$, the left- and right- hand polarized beams are exhibited orderly from left to right. The second row shows the simulation results, while the third and fourth rows show that of $m = -1$, $n = 1$, and $\varphi_0 = \pi/4$.

Figure 3 shows the displacement of the stripes in the upper and bottom regions and the slope of the stripes in the middle agrees well with our theory. All the fringes have the same period of $\tau_x = b\lambda/a$ in the x-direction, but the stripes in the upper region have one order displacement to the left for the −1 order diffraction light and that is to the right for the +1 order. The polarization singularity in the middle region leads to the slope of the fringes in σ_2 region and the inclined stripes connect the vertical stripes in the upper and bottom region. The single-slit diffraction field is the superposition of that with the left- and right-hand polarized beams. Besides, the single-slit diffraction patterns of the arbitrary vector beams are only related to the topological charge m.

Figure 4 shows the experimental and simulation results for the complex vector beams with $m = 2$, $n = 0$, $\varphi_0 = 0$, and $m = 3$, $n = 0$, $\varphi_0 = 0$. The diffraction patterns become complicated especially in the middle region with the increase in m, the total intensity matches well with the superposition of that of the ±1 order beams. In the center, the diffraction pattern exhibits a chessboard structure, because they are the superpositions of the slope stripes in the center of the −1 and +1 order diffraction lights. In

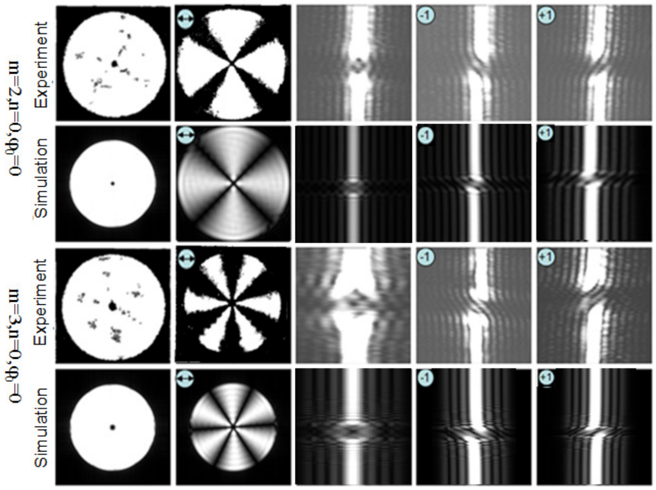

Fig. 4. Experimental and simulation results of the single-slit diffraction patterns of vector field with $m = 2$, $m = 3$, $n = 0$, $\varphi_0 = 0$.

other words, there are periodic bright and dark stripes both in the x- and y-directions in σ_2 region, and the number of the bright and dark fringes in the y-direction is $2m$–1. It is bright in the center when m is even as shown in the first row, whereas it is dark when m is odd as shown in the third row.

Figures 3 and 4 show that the single-slit diffraction fields only comply with the topological charge m and the other parameters n and φ_0 do not work. But these parameters play a very important role in the distribution of the polarization, so we explore the polarization distribution of single-slit diffraction fields of the arbitrary vector beams with different m, n, φ_0. Figure 5(a) shows the distribution of the polarization of the vector beams with $m = 1$, 2, and 3, $n = 0$, $\varphi_0 = 0$ and Fig. 5(b) shows the simulation results.

As shown in Fig. 5, the diffraction patterns of the vector fields exhibit the spatial structure in the x- and y-(slit) directions described by I_x and I_y. The x-component of the diffraction patterns is discussed firstly. For the first row, $I_x = I_{-1}\times\cos^2(\pi/2)+I_{+1}\times\cos^2(-\pi/2) = 0$ in σ_1, and $I_x = I_{-1}\times\cos^2(3\pi/2)+I_{+1}\times\cos^2(-3\pi/2) = 0$ in σ_3, so there is no fringe in these regions. But in σ_2, I_x can be given as $I_x^{(y=y_0)} = c^{(y=y_0)}\times I\times\cos^2\theta^{(x=b/2,y=y_0)}$. Therefore, θ is from π to $\pi/2$ when y is from 0 to ∞, then I_x is from I to 0. This trend is contrary to the periodicity of the central column fringe in the y-direction, but complies with the next columns, so the fringes of only odd number columns are retained. For the y-component, $I_y = I_{-1}\times\sin^2(\pi/2)+I_{+1}\times\sin^2(-\pi/2) = I$ in σ_1 and $I_y = I_{-1}\times\sin^2(3\pi/2)+I_{+1}\times\sin^2(-3\pi/2) = I$ in σ_3, so the fringes of I_y are the same with that of I. In σ_2, $I_y^{(y=y_0)} = c^{(y=y_0)}\times I\times\sin^2\theta^{(x=b/2,\,y=y_0)}$, so I_y is from 0 to I when y is from 0 to ∞. This trend is contrary to the periodicity of the even number columns fringe, but complies with the next columns, so the fringes of only even number columns are retained which are the dark fringes in this region. That means no fringe in this region.

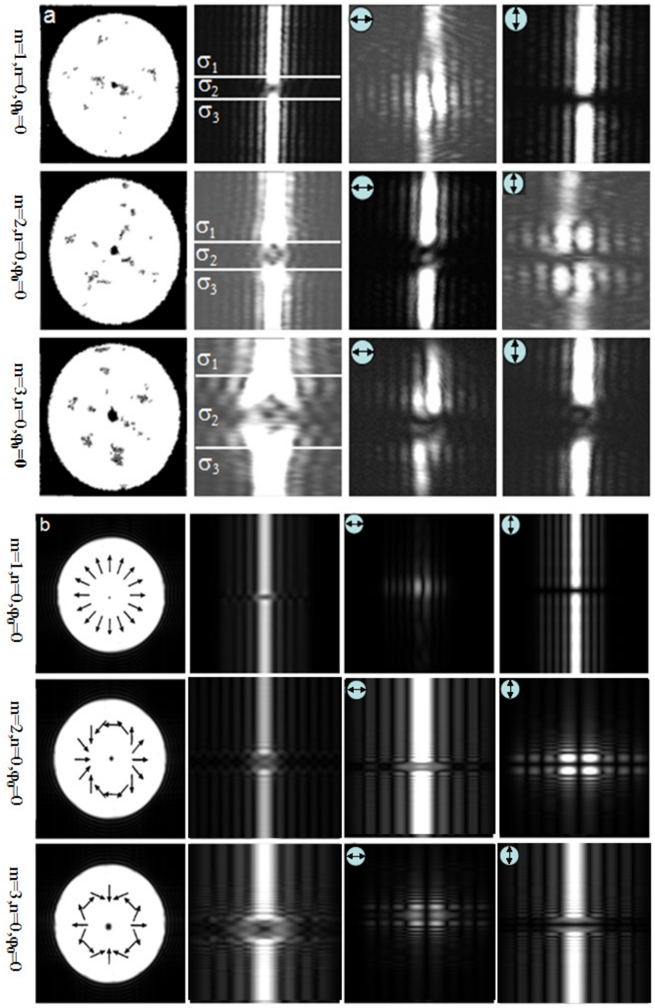

Fig. 5. (a) Experimental results of the single-slit diffraction patterns of vector field with $m = 1$, 2, 3, $n = 0$, $\varphi_0 = 0$, and (b) simulation of the single-slit diffraction patterns of vector field with $m = 1$, 2, 3, $n = 0$, $\varphi_0 = 0$. The right columns show the distribution of the x- and y- components.

For the vector beam with $m = 2$ as the second row in Fig. 5, $I_x = I_{-1}\times\cos^2(0) + I_{+1}\times\cos^2(0) = I$ in σ_1 and $I_x = I_{-1}\times\cos^2(2\pi)+I_{+1}\times\cos^2(-2\pi) = I$ in σ_3, so I_x is the same with I. In σ_2, $I_x^{(y=y_0)} = c^{(y=y_0)}\times I\times\cos^2\theta^{(x=b/2,y=y_0)}$, θ is from 2π to π when y is from 0 to ∞, then I_x is from I to 0 to I. This trend is contrary to the periodicity of the even number columns fringes and complies with the next column. As a result, the fringes of only even number columns are retained in this region. For the y-component, $I_y = I_{-1}\times\sin^2(0) + I_{+1}\times\sin^2(0) = 0$ in σ_1, and $I_y = I_{-1}\times\sin^2(2\pi)+I_{+1}\times\sin^2(-2\pi) = 0$ in σ_3, therefore there is no fringe. In σ_2, $I_y^{(y=y_0)} = c^{(y=y_0)}\times I\times\sin^2\theta^{(x=b/2,\,y=y_0)}$, in the same way, I_y is from 0 to I to 0 when y is from 0 to ∞. Therefore the trend is contrary to that of the x-component, so the fringes of only odd number columns are retained in this region.

We can deduce that there is no fringe for the x-component in σ_1 and σ_3 when m is odd. But in σ_2, the fringes of only odd number columns will be retained and the number of the bright and dark fringes in the y-direction is $2m - 1$. For the y-component, I_y is the same with I in σ_1 and σ_3, but in σ_2, the fringes of only even number columns will be retained and the number of the bright and dark fringes in the y-direction is also $2m - 1$. However, when m is even, I_x will swap with I_y. The last row of Fig. 5 proves our analysis very well.

Figure 6 shows the diffraction patterns and the polarization distribution of the vector beams are $m = 1$, $n = 0$, and $\varphi_0 = 0$, $\pi/4$, $2\pi/4$, $3\pi/4$. The diffraction patterns of vector light fields exhibit different spatial structures as different φ_0. The first row in Fig. 6 is same as Fig. 5 and has been analyzed. For the second row with $\varphi_0 = \pi/4$, $I_x = I_{-1}\times\cos^2(\pi/4) + I_{+1}\times\cos^2(-\pi/4) = I/2$ in σ_1 and $I_x = I_{-1}\times\cos^2(5\pi/4) + I_{+1}\times\cos^2(-5\pi/4) = I/2$ in σ_3. As a result, I_x is the same as I with certain weak intensity. In the σ_2 region

$$I_x^{(y=y_0)} = c^{(y=y_0)} I \cos^2\left(\theta + \frac{\pi}{4}\right) + \cos^2\left(-\theta + \frac{\pi}{4}\right) = c_1^{(y=y_0)} I, \tag{13}$$

where θ is the polarizing angle when $\varphi_0 = 0$. So fringes of I_x remain that of I.

For the y-component, $I_y = I_{-1}\times\sin^2(\pi/4) + I_{+1}\times\sin^2(-\pi/4) = I/2$ in σ_1 and $I_y = I_{-1}\times\sin^2(5\pi/4) + I_{+1}\times\sin^2(-5\pi/4) = I/2$ in σ_3. In the σ_2 region

$$I_y^{(y=y_0)} = c^{(y=y_0)} I \left(\sin^2\left(\theta + \frac{\pi}{4}\right) + \sin^2\left(-\theta + \frac{\pi}{4}\right)\right) = c_2^{(y=y_0)} I, \tag{14}$$

which is the same as I_x. The vector beam with $m = 1$, $n = 0$, $\varphi_0 = 3\pi/4$ is the same as shown in the fourth row. In fact, according to the calculated process, we can deduce that the results of vector beam with $m = 1$, $n = 0$, $\varphi_0 = m\pi/2 + \pi/4$ will all be the same.

The third row of Fig. 6 shows the results of vector beam with $m = 1$, $n = 0$, $\varphi_0 = 2\pi/4$. $I_x = I_{-1}\times\cos^2(\pi) + I_{+1}\times\cos^2(\pi) = I$ in σ_1 and $I_x = I_{-1}\times\cos^2(2\pi) + I_{+1}\times\cos^2(-2\pi) = I$ in σ_3, so the fringes in these regions are the same as that of I. But in σ_2 region,

$$\begin{aligned} I_x^{(y=y_0)} &= c^{(y=y_0)} I \left(\cos^2\left(\theta + \frac{\pi}{2}\right) + \cos^2\left(-\theta + \frac{\pi}{2}\right)\right) \\ &= c_1^{(y=y_0)} I \cos^2\theta, \end{aligned} \tag{15}$$

where θ is from π to $3\pi/2$ when the y is from 0 to ∞, which is the same with I_y in the first row. So I_x with $m = 1$, $n = 0$, $\varphi_0 = 2\pi/4$ is the same with the I_y with $m = 1$, $n = 0$, $\varphi_0 = 0$. Furthermore, I_y with $m = 1$, $n = 0$, $\varphi_0 = 2\pi/4$ is the same with I_x with $m = 1$, $n = 0$, $\varphi_0 = 0$, which is shown in the first and third rows of Fig. 6. Besides, we can deduce that the polarization distribution is one cycle of vector beams with φ_0 from 0 to π (Fig. 6).

Lastly, the polarization distribution of vector beams with different n is discussed. Figure 7(a) shows the diffraction patterns and the polarization distribution of vector beams with $m = 1$, $\varphi_0 = 0$ and different n where $n = 0.5$, 1, 1.5 and Fig. 7(b) shows the simulation results.

As shown in Fig. 7, the diffraction patterns exhibit the spatial periodicity structure in the y-(slit) direction when δ changes as radius. Because the phase $2n\pi\rho/\rho_0$ can be supposed to be uniform from left to right, the change in the phase distribution is only in the vertical direction. In the upper half portion, $I_x = I_{-1}\times\cos^2(\pi\rho/\rho_0) + I_{+1}\times\cos^2(-\pi\rho/\rho_0) = I\times\cos^2(\pi\rho/\rho_0)$. In the bottom portion, $I_x = I_{-1}\times\cos^2(-\pi\rho/\rho_0) + I_{+1}\times\cos^2(\pi\rho/\rho_0) = I\times\cos^2(\pi\rho/\rho_0)$. θ is from 0 to π when y is from 0 to ρ_0, then I_x is from I to 0 to I which is n periodic change in the y-direction.

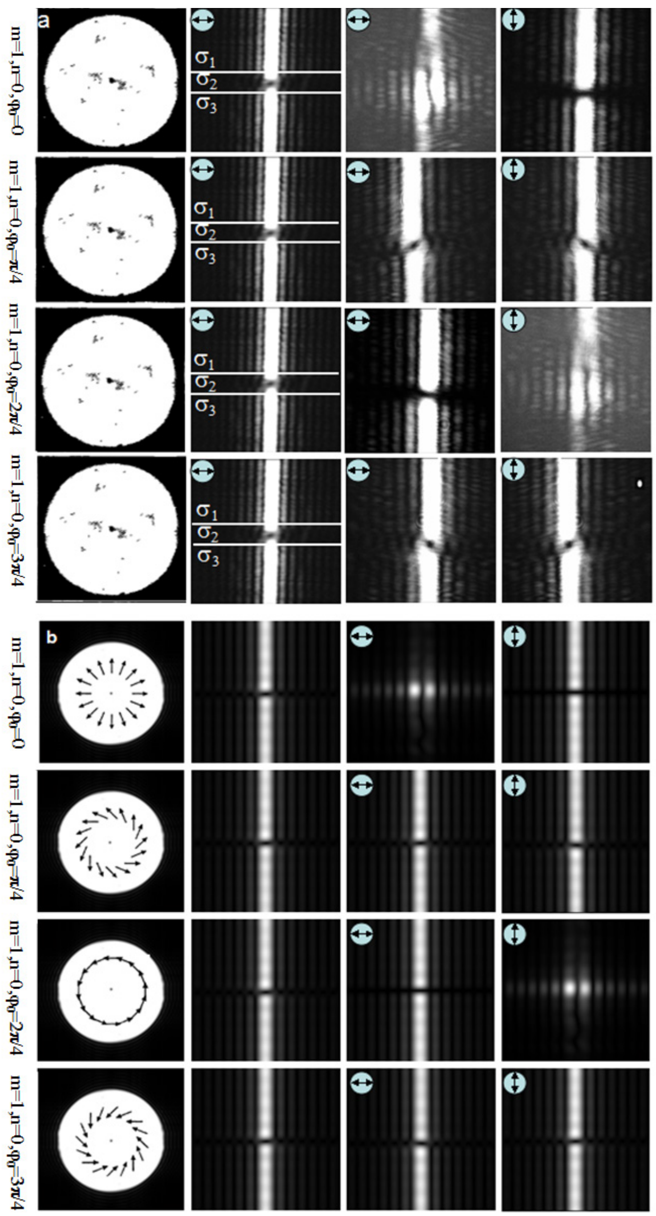

Fig. 6. (a) Experimental results of the single-slit diffraction patterns with vector beam with $m = 1$, $n = 0$, $\varphi_0 = 0$, $\pi/4$, $2\pi/4$, $3\pi/4$ and (b) simulation results of the single-slit diffraction patterns with vector beam with $m = 1$, $n = 0$, $\varphi_0 = 0$, $\pi/4$, $2\pi/4$, and $3\pi/4$.

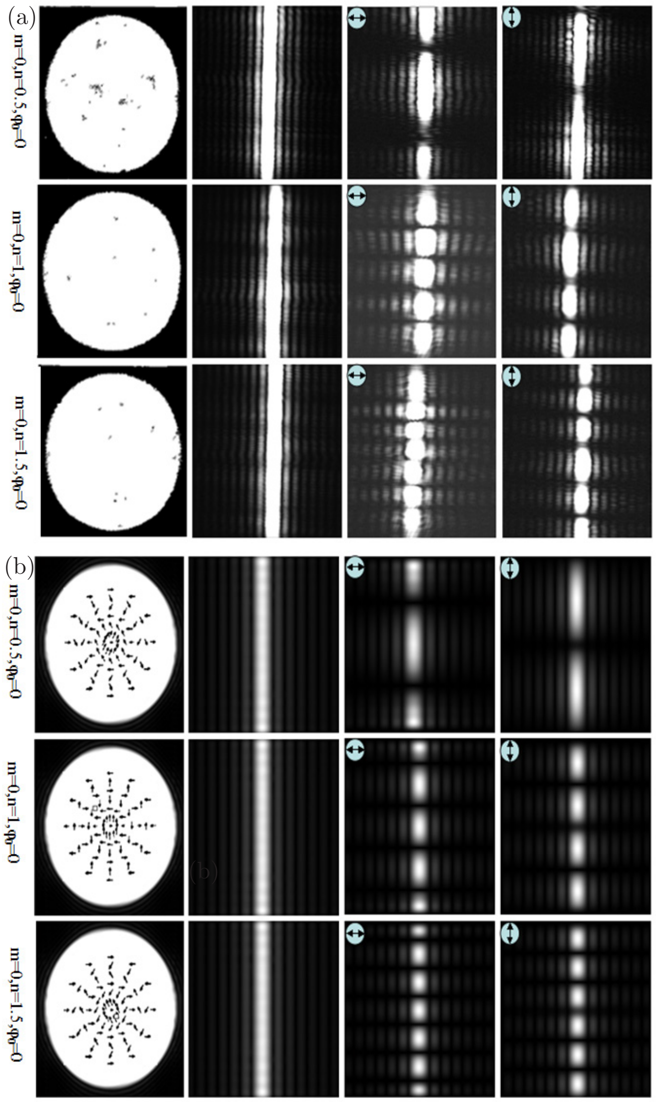

Fig. 7. (a) Experimental results of the single-slit diffraction patterns with vector beam with $m = 1$, $\varphi_0 = 0$, $n = 0.5$, 1, 1.5 and (b) simulation results of the single-slit diffraction patterns with vector beam with $m = 1$, $\varphi_0 = 0$, $n = 0.5$, 1, 1.5.

The center is bright and in the bottom it is the same. For the y-component, in the upper half portion, $I_y = \mathrm{I}_{-1}\times\sin^2(\pi\rho/\rho_0) + I_{+1}\times\sin^2(-\pi\rho/\rho_0) = I\times\sin^2(\pi\rho/\rho_0)$, so I_y is from 0 to I to 0, so there is also n cycles periodic change in the y-direction but the center is dark, and it is the same in the bottom. Furthermore, it is the same with $n = 1.5$, 2 as shown in the second and third rows of Fig. 7. We can draw the conclusion that the phase $2n\pi\rho/\rho_0$ does not contribute to the total intensity of the single-slit diffraction but will change both the x- and y-components to be periodical which is $2n$ cycles. The fringe is bright in the center for I_x while it is dark for I_y when m is odd, and that is opposite when m is even.

In conclusion, we present single-slit diffraction of the arbitrary vector fields with different parameters m, n, and φ_0 theoretically and experimentally. The single slit covers the polarization singularity in the center. Firstly, we figure out the relationship between the diffraction patterns and the parameters m, n, and φ_0. In particular, the influence of the polarization singularity on the diffraction fringes is analyzed. The total intensity of the diffraction field is related only to the topological charge m, but the polarization distribution of the diffraction field is related to all the parameters m, n and φ_0. Therefore, the diffraction patterns allow to determine all the parameters of the arbitrary vector fields. The experimental results agree well with the simulation results. In addition, our research on the phenomenon of vector near-field diffraction has a guiding significance for the study of the spatial and temporal evolutions of the vector optical field and the interaction of vector light with matter.

This work was supported by the National Natural Science Foundation of China under Grant No. 61275133.

References

1. Y. Q. Zhao, J. S. Edgar, G. D. M. Jeffries, D. McGloin, and D. T. Chiu, Phys. Rev. Lett. **99,** 073901 (2007).
2. F. Lu, W. Zheng, and Z. Huang, Opt. Lett. **34,** 1870 (2009).
3. P. Y. Chiou, A. T. Ohta, and M. C. Wu, Nature **436,** 370 (2005).
4. T. Duan, C. Jin, and C. Li, Chin. Opt. Lett. **09,** S10602 (2011).
5. X. L. Wang, J. P. Ding, W. J. Ni, C. S. Guo, and H. T. Wang, Opt. Lett. **32,** 3549 (2007).
6. X. Jia, B. Li, and Y. Wang, Chin. Opt. Lett. **8,** 517 (2010).
7. S. Sato and Y. Kozawa, Opt. Lett. **34,** 3166 (2009).
8. A. A. Ishaaya, L. T. Vuong, T. D. Grow, and A. L. Gaeta, Opt. Lett. **33,** 13 (2008).
9. J. T. Barreiro, T. C. Wei, and P. G. Kwiat, Phys. Rev. Lett. **105,** 030407 (2010).
10. W. Chen and Q. Zhan, Opt. Lett. **34,** 722 (2009).
11. Y. G. Li, X. L. Wang, H. Zhao, L. J. Kong, B. Gu, C. Tu, and H. T. Wang, Opt. Lett. **37,** 1790 (2012).
12. Y. M. Luo, B. D. Li, B. H. Tang, and Y. Zhu, Acta Phys. Sin. **13,** 134202 (2012).
13. M. S. Soskin, V. G. Denisenko, and R. I. Egorov, Proc. SPIE **80,** 17 (2004).
14. K. Y. Bliokh, A. Niv, V. Kleiner, and E. Hasman, Opt. Express **80,** 16695 (2008).
15. P. S. Liu and B. D. Lü, Opt. Laser. Technol. **40,** 227 (2008).
16. M. V. Berry and M. R. Dennis, Proc. R. Soc. Lond. **457,** 141 (2001).
17. M. R. Dennis, Opt. Commun. **213,** 201 (2008).
18. J. Masajada, Opt. Commun. **175,** 289 (2000).
19. L. Guo and Z. Tang, Chin. Opt. Lett. **10,** S10601 (2012).
20. G. V. Bogatyryova, C. V. Felde, S. A. Ponomarenko, M. Soskin, and E. Wolf, Opt. Lett. **28,** 878 (2003).
21. H. I. Sztul and R. R. Alfano, Opt. Lett. **31,** 999 (2006).
22. D. P. Ghai, P. Senthilkumaran, and R. S. Sirohi, Opt. Lasers Eng. **47,** 123 (2009).
23. V. V. Kotlyar, S. N. Khonina, A. A. Kovalev, V. A. Soifer, and H. Elfstrom, J. Opt. Lett. **31,** 1597 (2006).
24. V. Pyragaite and A. Stabinis, Opt. Commun. **213,** 187 (2008).
25. C. Hnatovsky, V. Shvedov, W. Krolikowski, and A. Rode, Phys. Rev. Lett. **106,** 123901 (2011).